Chaos, Solitons and Fractals 196 (2025) 116353

Contents lists available at ScienceDirect

Chaos, Solitons and Fractals

journal homepage: www.elsevier.com/locate/chaos

Josephson "flying qubit" revival: Flux-based control optimization

M.V. Bastrakova [a,b,*], D.S. Pashin [a], P.V. Pikunov [a], I.I. Soloviev [c,d], A.E. Schegolev [c], N.V. Klenov [e]

[a] Faculty of Physics, Lobachevsky State University of Nizhni Novgorod, Nizhny Novgorod, 603022, Russia
[b] Russian Quantum Center, Skolkovo, Moscow, 143025, Russia
[c] Skobeltsyn Institute of Nuclear Physics, Lomonosov Moscow State University, Moscow, 119991, Russia
[d] Moscow Institute of Physics and Technology, Dolgoprudny, 141700, Russia
[e] Faculty of Physics, Lomonosov Moscow State University, Moscow, 119991, Russia

ARTICLE INFO

Keywords:
Adiabatic quantum flux parametron
Landau–Zener transitions
Flying qubits
Magnetic flux control
Superconducting circuits
Nonlinear dynamics

ABSTRACT

A decade ago, Josephson "flying qubits" based on adiabatic superconducting logic cells showed promise as quantum data buses, but their development stalled due to the incompatibility of traditional qubit control methods with their design. We revisit this concept by exploring the control of the inductively shunted two-junction superconducting interferometer (adiabatic quantum flux parametron, AQFP) in the quantum regime using unipolar magnetic field pulses generated by adiabatic superconducting electronics. Our research demonstrates the feasibility of high fidelity quantum operations (fidelity more than 99.99%) in this system via Landau–Zener tunneling. To this end, a method is proposed for selecting the duration and shape of control pulses to eliminate unwanted leakage into high-lying states in AQFP-based systems.

1. Introduction

Recent years have seen a resurgence of interest in Josephson flux-based qubits and quantum circuits due to the relatively long decoherence times and pronounced anharmonicity of the energy spectrum [1–7]. At the same time, challenges with the implementation of inter-qubit interactions in such systems and the transfer of data between blocks are still relevant. On the other hand, classical digital Josephson devices with information in the magnetic flux domain are also actively developed. In particular, several variants of the basic cell for adiabatic superconducting logic (ASL) based on the parametric quantron [8–12] for arithmetic-and-logic [13–16] and neuromorphic applications [17–23] were proposed. Of particular interest is the penetration of ASL-based technical solutions into the field of quantum technologies for qubit control and quantum state readout [24–26].

When we discuss logic operations using ASL circuits, it is worthwhile to first consider the basic cell: a superconducting ring with two weak links called Josephson junctions and an additional superconducting shunt. In terms of the physical basis of logic operations, this is a circuit with several reactive elements that allows oscillation processes in two different modes, symbolizing logic "0" and "1". These two different modes correspond to the directions of the circulating currents in the loops of this parametron-like cell. In order to maintain continuity, the cell is designated as an adiabatic quantum flux parametron (AQFP) [8,9,11].

The potential energy of such a cell consists of the Josephson energy and the magnetic energy. By adjusting the current and the magnetic field, one can control the shape of the potential energy profile U_M. The dependence of the potential energy on the generalized coordinate (Josephson phase) is close to the "parabolic" shape and could have one or two minima with respect to the external parameters.

The transmission of information in classical ASL data buses is realized by the magnetic coupling of their contours during the sequential activation of cells. In logic circuits, cells are periodically activated under the influence of an external (clock) signal that causes activation (i.e. the change from a single-well to a double-well shape of the potential energy profile).

The implementation of Josephson data transfer buses in quantum mode is an urgent scientific and technical problem. And one of the attempts to solve it is the creation of "flying qubits" based on soliton-like excitations in Josephson systems [27–33]. We believe that a chain of AQFP cells [34–39] can be considered as the basis for a practical implementation. This belief is based on the achievability of logical (one can reconstruct the input from the output) and physical (except for energy dissipation during the logic operation) reversibility of classical computing in such systems [38]. In addition, the AQFP-based cell can operate at ultra-low temperatures (milliKelvin) while maintaining quantum coherence [7].

* Corresponding author at: Faculty of Physics, Lobachevsky State University of Nizhni Novgorod, Nizhny Novgorod, 603022, Russia.
E-mail address: bastrakova@phys.unn.ru (M.V. Bastrakova).

https://doi.org/10.1016/j.chaos.2025.116353
Received 27 December 2024; Received in revised form 19 February 2025; Accepted 20 March 2025

The concept of flying qubits based on Josephson qubits for data buses was proposed more than a decade ago [40,41], but their design development stalled until recently due to the complexity of the state management systems. A particular issue is the creation of a quantum data bus control system that allows data to be transferred without loss of information. Traditional microwave technology with relatively large superconducting resonators is poorly compatible with relatively large AQFP-based circuits: as the number of qubits increases, crosstalk problems arise whose suppression requires the control and fine-tuning of multiple resonators. A solution to this problem can be found in controlling selected AQFPs in the quantum regime using classical ASL circuits, since such quantum data buses (chains of coupled AQFPs) can be realized on a high-density chip, while resonators require significantly more physical space [42].

The key idea of our work is the study of the AQFP-based qubit drive with unipolar and relatively long magnetic flux pulses, which can be obtained from the output of a classical AQFP cell. In working with quantum information, it is also possible to optimize the shape of the control flux entering the AQFP and implement an analog of quantum data buses.

2. Model of the basic adiabatic cell with magnetic flux control

Let us take a closer look at the scheme of the two Josephson junction superconducting interferometer with inductive shunting (see Fig. 1a), which we propose to use as the main cell for the implementation of a "flying" qubit. This is essentially an AQFP circuit, where the external bias is denoted as a shift current i_{shift} inducing a phase φ_{shift} across the shunt inductor l_{out}. The case of a symmetric AQFP scheme, where the arms containing Josephson junctions are identical [26], is well studied in the literature. We consider the possibility of variations in the characteristics of the interferometer arms containing Josephson junctions. The mismatch of inductance values is often caused by the experimental fabrication process and must be taken into account since it introduces an asymmetry of the magnetic flux penetration into the contours of the interferometer circuit. The control signal $\varphi_{in_{1,2}}(t)$ is applied through the inductive arms $l_{1,2}$ of the interferometer. Fig. 1b shows the idea visualization of the AQFP-based quantum data bus for transmitting a logical state using the example of a simple magnetically coupled chain.

The potential energy of the system is governed by two main components: control current and shift current.

(1) Control current lines $i_{in_{1,2}}$ are magnetically coupled to each of the inductive arms with inductances $l_{1,2}$. These current lines are responsible for synchronization of interferometer operations with neighboring cells in the quantum data bus.

(2) A separate shift line i_{shift} is galvanically connected to the AQFP circuit at the convergence point of the arms ($l_{1,2}$ and l_{out}). This line is used to define the adiabatic evolution direction for the potential energy of the cell; it could also be used as an additional valve to fine-tune the effective difference of the circulating currents in the cell circuits. The mutual direction of the currents circulating in these circuits determines the logical state of the AQFP: if the currents are unidirectional – it corresponds to a logical "0", if they are bidirectional – it corresponds to a logical "1".

This scheme provides adiabatic control of the system states, allowing the application of magnetic flux pulses. In our consideration, we used a smooth trapezoidal shape as a realistic model of an impact for the AQFP cell:

$$\varphi_{in_j}(t) = A_j \left(\left(1 + e^{-2D_j(t-t_1)}\right)^{-1} + \left(1 + e^{2D_j(t-t_2)}\right)^{-1} \right), \tag{1}$$

where the parameters A_j and D_j set the level and the rise/fall rate of the magnetic flux input to the quantum AQFP, respectively, and the index $j = 1, 2$ corresponds to the number of the current control line i_{in_j}. We assume that the external magnetic flux is normalized to the magnetic flux quantum, $\Phi_0 = \frac{h}{2e}$.

To illustrate the idea of the AQFP functionality, we have shown in Figs. 1c-e the view of the symmetric interferometer (the case when Josephson junctions have the same characteristics: critical currents and capacities are equal $I_{c_1} = I_{c_2} = I_c$ and $C_1 = C_2 = C$, and the interferometer shoulder inductances are also equal $l_1 = l_2 = l$) potential energy during its evolution as the control phase φ_{in} varies from zero to π. The presence of a non-zero shift current determines the asymmetry of the potential at rest (determining the direction of the subsequent evolution of the system), when the control signal φ_{in} is set to zero. The change of the control signal triggers the evolutionary process by changing and shifting the energy profile of the AQFP U_{total}:

$$U_{total} = \frac{(\varphi_{shift} - \theta)^2}{l + 2l_{out}} + \frac{(\varphi_{in} + \psi)^2}{l} - 2\cos\theta\cos\psi, \tag{2}$$

where $\varphi_{shift} = i_{shift} \cdot l_{out}$, $\theta = (\varphi_1 + \varphi_2)/2$ and $\psi = (\varphi_1 - \varphi_2)/2$ are the designations of the half-sum and half-difference of phases $\varphi_{1,2}$ on the Josephson junctions $JJ_{1,2}$, respectively.

Figs. 1f-h show the potential cross sections along the sum phase axis θ/π at a fixed difference phase ψ_{min}, i.e. $U_{total}(\theta, \psi_{min})$, corresponding to the potential energy minimum (marked with a red dot). Additional black arrows show the direction of the potential shift (evolution) from the state corresponding to logic "0" to the state corresponding to logic "1". The corresponding switching between states due to the evolution of potential energy occurs along nearly equipotential trajectories. This ensures that there are no large voltage peaks at the Josephson contacts (nor transitions to a resistive state) and low (in the adiabatic limit is zero) energy dissipation per operation. Within the framework of this article, all energies are normalized to a characteristic Josephson energy value $E_J = \frac{\hbar I_c}{2e}$, where $I_c = I_{c_1} = I_{c_2}$ is the critical current of Josephson junctions.

Next, we consider a generalized AQFP model with asymmetric interferometer arms containing Josephson junctions, when $I_{c_1} \neq I_{c_2}$, $l_1 \neq l_2$, $C_1 \neq C_2$. A complete description of the dynamics of the system shown in Fig. 1a requires a joint solution of Kirchhoff's equations and the equations of phase balance in superconducting circuits:

$$\begin{cases} i_1 + i_2 + i_{out} = i_{shift}, \\ \varphi_1 + l_1 i_1 + \varphi_{in_1} = i_{out} l_{out}, \\ \varphi_2 + l_2 i_2 - \varphi_{in_2} = i_{out} l_{out}. \end{cases} \tag{3}$$

Here $\varphi_{1,2}$ are the Josephson phases at the junctions $JJ_{1,2}$, which act as generalized coordinates for the considered pair of coupled nonlinear oscillators. All currents are normalized to the critical current of the first Josephson junction I_{c_1}, and inductances — to the characteristic value $\frac{\Phi_0}{2\pi I_{c_1}}$.

The solution of the system (3) shows that the currents in the considered model depend linearly on the phases of the Josephson junctions and the external currents:

$$i_j = k^{(j)}_{\varphi_1}\varphi_1 + k^{(j)}_{\varphi_2}\varphi_2 + k^{(j)}_{\varphi_{in_1}}\varphi_{in_1} + k^{(j)}_{\varphi_{in_2}}\varphi_{in_2} + k^{(j)}_{\varphi_{shift}}\varphi_{shift}. \tag{4}$$

The coefficients in (4) for each Josephson junction current ($j = 1, 2$) are found from the solution of the system (3) and have the following form:

$$k^{(1)}_{\varphi_1} = k^{(1)}_{\varphi_{in_1}} = -\frac{l_2 + l_{out}}{l_1 l_2 + l_{out}(l_1 + l_2)},$$

$$k^{(1)}_{\varphi_2} = k^{(2)}_{\varphi_1} = k^{(2)}_{\varphi_{in_1}} = -k^{(1)}_{\varphi_{in_2}} = \frac{l_{out}}{l_1 l_2 + l_{out}(l_1 + l_2)},$$

$$k^{(2)}_{\varphi_2} = -k^{(2)}_{\varphi_{in_2}} = -\frac{l_1 + l_{out}}{l_1 l_2 + l_{out}(l_1 + l_2)},$$

$$k^{(1)}_{\varphi_{shift}} = \frac{l_2}{l_1 l_2 + l_{out}(l_1 + l_2)},$$

$$k^{(2)}_{\varphi_{shift}} = \frac{l_1}{l_1 l_2 + l_{out}(l_1 + l_2)}.$$

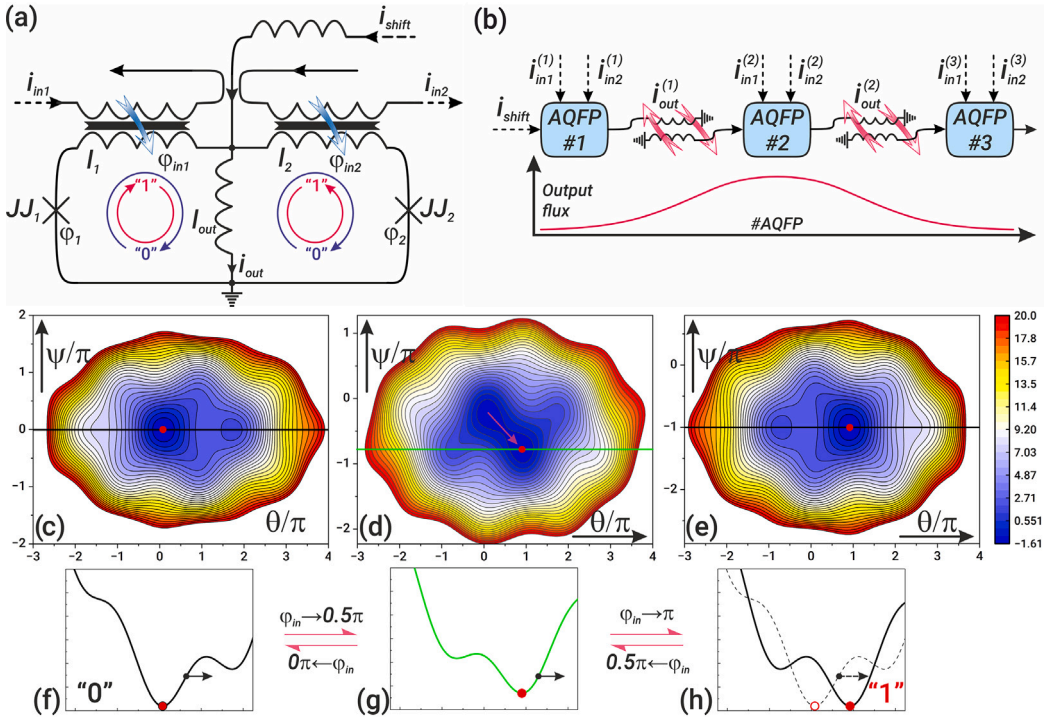

Fig. 1. (a) Schematic of an adiabatic quantum flux parametron (AQFP) with control ($i_{in1,2}$) and shift (i_{shift}) lines. φ_1 and φ_2 are phases of the Josephson junctions JJ_1 and JJ_2 in the AQFP, respectively. (b) Visualization of the idea of an AQFP-based quantum data bus for logic state transfer. Each AQFP cell has its own input control lines $i^{(k)}_{in_{1,2}}$, where k is the number of the corresponding AQFP in the data bus. (c) - (e) Potential energy of the symmetric AQFP ($l_1 = l_2 = l = 1.4$, $l_{out} = 1.9$, $\varphi_{in_1} = \varphi_{in_2} = \varphi_{in}$, $\varphi_{shift} = 0.5\pi$) versus the half-sum, θ, and half-difference, ψ, Josephson phases divided by π at $\varphi_{in} = 0; 0.5\pi; \pi$. (f) - (h) Potential energy cross-sections, corresponding to (c)–(e) show the slice of the potential passing through its minimum value at a fixed difference phase ψ, $U_{total}(\theta/\pi, \psi_{min}/\pi)$. The positions of the minima of the potential at the corresponding φ_{in} are marked by red circles. The red arrow in figure (d) shows the direction of the adiabatic evolution of the system along the "valley" of the potential during the transition from the initial state (logical "0") to the final state (logical "1") through the intermediate state. Black arrows indicate the direction of potential evolution. Energy U_{total} is normalized to the characteristic Josephson energy E_J.

The current through the Josephson junction $JJ_{1,2}$ could be described using Josephson relations and the laws of classical electrodynamics, assuming low losses and a simple current-phase dependence, as follows:

$$i_j = c_j \ddot{\varphi}_j + i_{c_j} \sin \varphi_j, \tag{5}$$

where notations $c_j = C_j/C_1$ and $i_{c_j} = I_{c_j}/I_{c_1}$ are introduced for normalized capacitances and critical currents, and the dimensionless time is defined as $\tau = t/t_c$, where $t_c = \sqrt{\frac{\Phi_0 C_1}{2\pi I_{c_1}}}$, C_j are capacitances of each Josephson junction $j = 1, 2$. Note that we are focusing on studying the nonlinear dynamics of non-shunted Josephson junctions, which are used in the design of flux qubits [1,6,7].

Within the Hamiltonian formalism, we can write down the equations of motion and the Hamiltonian of the system if we introduce generalized momenta, which we denote as $p_j = c_j \dot{\varphi}_j$. The kinetic energy is determined by the capacitive contribution of Josephson junctions, which is calculated by the formula $\frac{p_j^2}{2c_j}$. The potential energy, in turn, depends on the inductive contributions, as was shown in Eq. (2):

$$U = \sum_{j=1,2} \left[\frac{k^{(j)}_{\varphi_j} \varphi_j^2}{2} + (k^{(j)}_{\varphi_{in_1}} \varphi_{in_1}(t) + k^{(j)}_{\varphi_{in_2}} \varphi_{in_2}(t) + k^{(j)}_{\varphi_{shift}} \varphi_{shift}) \cdot \varphi_j + i_{c_j} \cos \varphi_j \right] + k^{(1)}_{\varphi_2} \varphi_1 \varphi_2. \tag{6}$$

In order to study the nonlinear quantum dynamics of the AQFP, we applied the canonical quantization procedure in which the following substitution was performed: $\{\varphi_j, p_j\} \rightarrow -i[\hat{\varphi}_j, \hat{p}_j]$ (we use the units with $\hbar = 1$). This means performing a commutation relation on the operators $[\hat{\varphi}_j, \hat{p}_j] = i$. Then the generalized Hamiltonian of the system under consideration has the form:

$$\hat{H} = \sum_{j=1,2} \frac{\hat{p}_j^2}{2c_j} + \hat{U}. \tag{7}$$

3. The dynamics of the quantum system

Flux and fluxonium qubits are typically characterized by the isolation of a pair of basis states E_0 and E_1, which are separated by an energy gap from the overlying spectrum [1,4,43]. In this case, the realization of high-precision quantum operations is usually performed using microwave field pulses through high-quality resonators. However, this control technique is poorly compatible with data buses and adiabatic logic cells. Therefore, in this paper we study in detail the principles of magnetic flux control for the basic element of ASL logic in quantum mode of operation.

Magnetic flux pulses allow us to precisely control the potential energy dynamics, and hence the moments of energy level anticrossing, when quantum Landau–Zener tunneling between states can occur [44–46]. This effect is of recent interest for quantum control [47–52], since the Landau–Zener interference-based methodology is less sensitive to certain types of interference and allows to realize universal operations with high fidelity [53]. Consequently, such an approach first requires studying the behavior of the energy levels of the system depending on the external control field (1); in other words, we study the behavior of the instantaneous energy levels of the system (7), which can be found from equation:

$$\hat{H}|\psi_k\rangle = E_k|\psi_k\rangle, \tag{8}$$

where $|\psi_k\rangle$ and E_k are time-depending eigenfunctions and energies, corresponding to the kth eigenstate of the system.

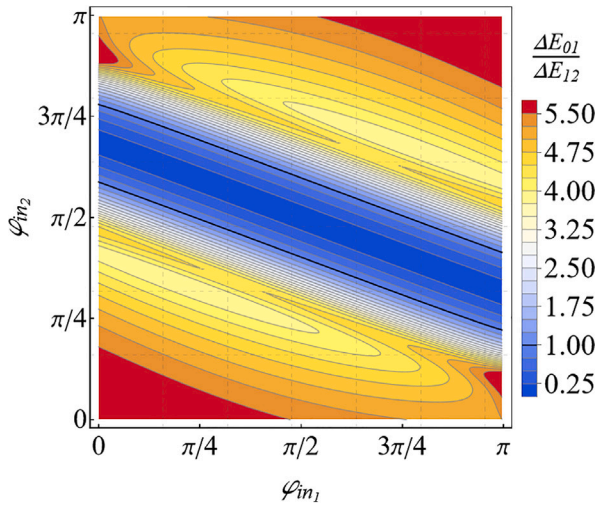

Fig. 2. The contour graph shows in color the ratio of the energy differences between the levels $\Delta E_{01}/\Delta E_{12}$ depending on the fluxes φ_{in_1} and φ_{in_2} at a constant phase shift value $\varphi_{shift} = \pi/2$. The black lines correspond to the cases where $\Delta E_{01}/\Delta E_{12} = 1$. Other system parameters: $l_1 = 1.98$, $l_2 = 1.82$, $l_{out} = 1.92$.

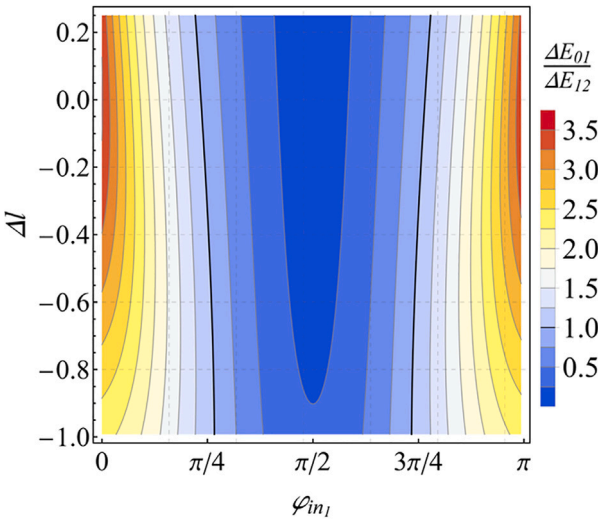

Fig. 3. The ratio of the energy difference as a function of the input flux φ_{in_1} and the inductance difference in the arms $\Delta l = l_2 - l_1$ at a constant value $\varphi_{shift} = \varphi_{in_2} = \pi/2$. The black lines correspond to the cases where $\Delta E_{01}/\Delta E_{12} = 1$. Other parameters: $l_1 = 1.98$, $l_{out} = 1.92$.

For the analysis of the spectrum and the selection of the qubit subspace (computation basis) the ratio of the energy difference between the main and the first excited levels $\Delta E_{01} = E_1 - E_0$ to the difference between the first and the second excited levels $\Delta E_{12} = E_2 - E_1$ is an important value. This value is colored in Fig. 2 for different external influences $\varphi_{in_{1,2}}$. At $\Delta E_{01}/\Delta E_{12} \ll 1$, the computational levels of the system are far away from the overlying spectrum (blue regions in Fig. 2), which allows us to isolate the system of lower states and consider it as a qubit. In the case of $\Delta E_{01}/\Delta E_{12} \gg 1$, the first excited level approaches the leakage level in the system, opening an additional escape channel from the computational subspace. In Fig. 2 the black lines correspond to the value $\Delta E_{01} = \Delta E_{12}$, which separates the two behavioral modes of the system levels. On the basis of this consideration it is possible to choose the external control for the effective selection of the operating point.

The nature of the AQFP energy spectrum shown in Fig. 2 allows one to fix the static magnetic flux through one of the control arms of the

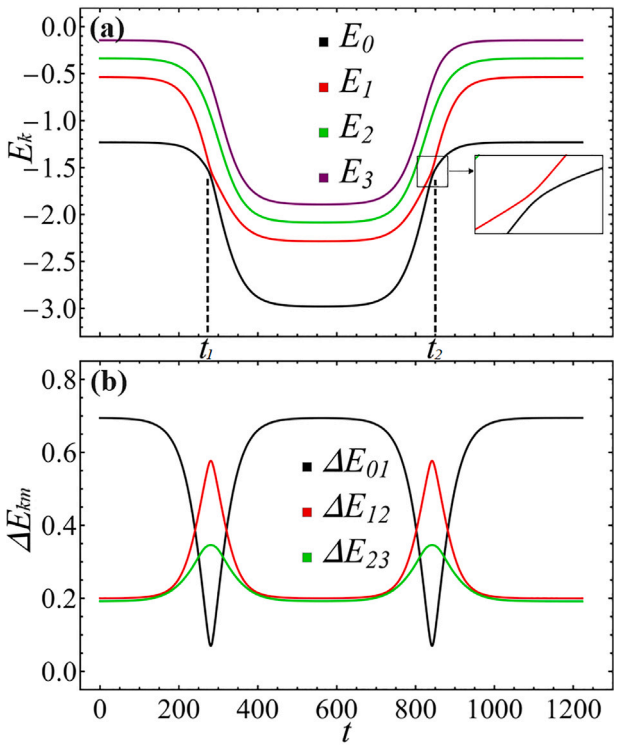

Fig. 4. The behavior of the low-lying energy levels E_k of the system (a) and their difference (b) as a function of time during signal transmission (1) at a constant value of $\varphi_{shift} = \varphi_{in_2} = \pi/2$. The other parameters are defined as follows: $l_1 = 1.98, l_2 = 1.802, l_{out} = 1.92$, $D_1 = 0.01425$, $t_1 = 280$, $t_2 = 842$. The dotted lines in figure (a) show the moments of level anticrossing corresponding to the times t_1 and t_2 in the control magnetic flux (1), and the black block indexes the behavior of levels E_0 and E_1 near their approach at t_2.

interferometer (for example, at JJ_2 by selecting the flux $\varphi_{in_2} = \pi/2$). At the same time, the basic levels become isolated from the rest of the overlying energy spectrum, i.e. $\Delta E_{01} \ll \Delta E_{12}$. Note that this trend in the spectrum persists for a fairly large range of arm inductors $\Delta l = l_2 - l_1$ at a fixed magnetic flux $\varphi_{in_2} = \pi/2$, as shown in Fig. 3. This allows us to implement a simple AQFP quantum dynamics control scheme with asymmetric arms ($\Delta l \neq 0$) using only a unipolar magnetic flux pulse of the form (1).

The dynamics of the instantaneous levels of the system is shown in Fig. 4. The levels behave adiabatically, except for the moments $t_{1,2}$ of rise and fall of the control signal when the instantaneous levels approach anticrossing. At these moments, non-pertubative Landau–Zener transitions occur [51,52], and this "tunneling" allows a transition between states, which manifests itself in a change in the dynamics of the level populations:

$$P_k = |\langle\psi(t)|\psi_k\rangle|^2. \tag{9}$$

Here $|\psi(t)\rangle$ is the state of the system found from the solution of the nonstationary Schrödinger equation.

Fig. 5a shows the behavior of the populations of low-lying AQFP levels when implementing the ground state inversion (the quantum operation of rotating the state vector on the Bloch sphere around the X axis) and (b) the behavior of leakage to an excited level outside the computational subspace of the qubit. The system was initialized in the ground state ($k = 0$). As a result of the unipolar effect, the system experiences two Landau–Zener transitions at the moments $t_{1,2}$ of the rise/fall of the magnetic flux, when the ground levels converge in the instantaneous basis, see Fig. 4. In the inset to Fig. 5a, the trajectory of the end of the state vector on the Bloch sphere is shown. It can be noted that at the time points between the transitions, free precession

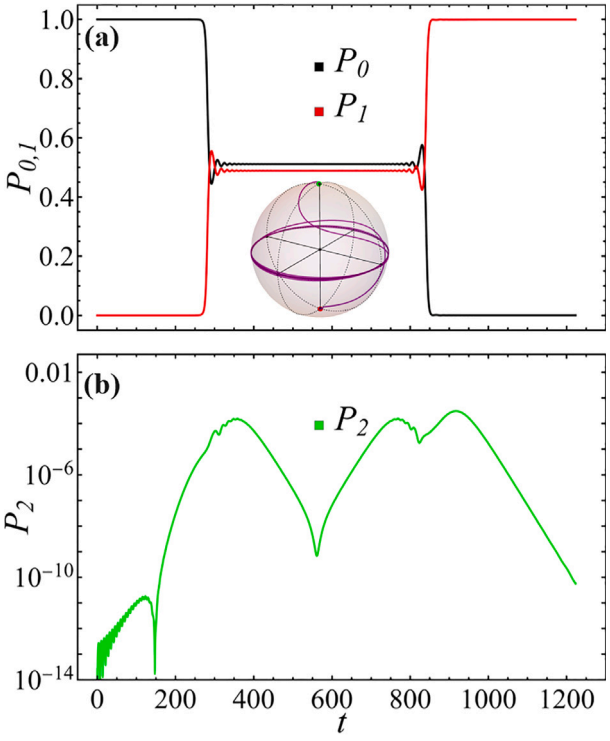

Fig. 5. Level population as a function of time during signal propagation at a constant value of $\varphi_{shift} = \varphi_{in_2} = \pi/2$ for operation X. At the initial time, the system was in the ground state at $k = 0$. Other parameters are: $l_1 = 1.98, l_2 = 1.802$, $l_{out} = 1.92$, $D_1 = 0.01425$, $t_1 = 280$, $t_2 = 842$.

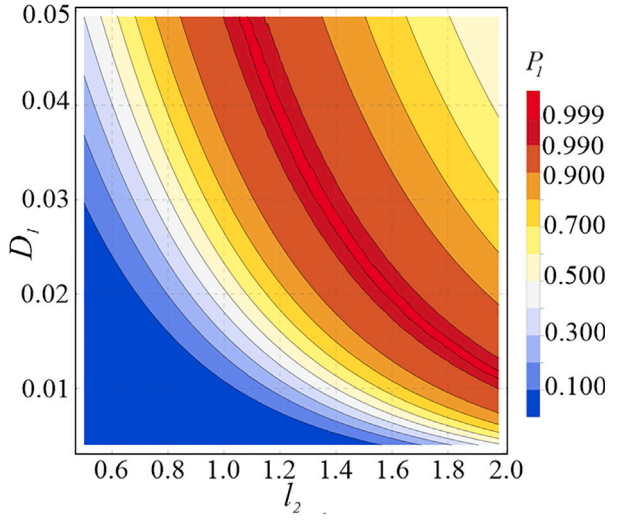

Fig. 6. The population of the first excited state at the end of the control signal exposure in depends on the parameters D_1 and l_2 with a constant value of $\varphi_{shift} = \varphi_{in_2} = \pi/2$. The parameter t_2 was varied to maximize the population of the first excited level. At the initial time, the system is initialized in the ground state $k = 0$. Other parameters are as follows: $l_1 = 1.98$, $l_{out} = 1.92$.

occurs in the azimuthal plane of the Bloch sphere with the frequency of the transition between the basic levels. Therefore for the correct execution of the quantum operation it is necessary to take into account the phase incursion, i.e. the time t_2 in the control action. Note that the energy structure of the levels in the system is such that the leakage into the overlying states of $k \geq 2$ does not exceed $P_2 \sim 10^{-4}$ near the convergence of the levels, and at the end of the external impact it even drops to the level of $P_2 \sim 10^{-8}$ (Fig. 5b). At the same time, the population inversion time (performing X rotation) is about 20 ns according to typical AQFP parameters ($I_{C_1} = 1\ \mu A$ and $C_1 = 10\ fF$).

The control of the nonlinear dynamics of the AQFP states in quantum mode is also possible by adjusting the parameters of the control external flux: the rise/fall rate of D_1 determines the characteristic tunneling time between states, and the times $t_{1,2}$ are responsible for adjusting the quantum phase. Optimization of these parameters is necessary for the implementation of high-precision quantum operations. One can see from Fig. 6 that it is possible to find optimal parameters for both the external control, D_1, and the system parameters, for example, the inductance l_2. The t_2 value was optimized based on the gradient descent method [54] to control the phase shift between the two Landau–Zener transitions, see the parameter map for the first excited level population (Fig. 6). Such an optimization procedure is necessary to control the quantum phase during the evolution from any initial state.

In Fig. 7 we demonstrate the importance of taking into account the relationships between the times of the Landau–Zener transitions to perform quantum operations for an arbitrary initial state, represented by a green dot on the Bloch sphere.

First, Fig. 7a shows that by varying only the value of the fall time t_2 of the signal, we can control the phase accumulated between Landau–Zener transitions (commonly known as the Stuckelberg phase [52]). However, this is not enough to implement an arbitrary quantum gate [53]. This is shown by a curve on the Bloch sphere (Fig. 7a), where the purple points represent the final state of the system after the unipolar action of φ_{in_1}. Even if we take into account the arbitrary rotation around the z axis, there are still regions of unreachable states near the poles of the Bloch sphere. This is demonstrated by the location of the points in Fig. 7b corresponding to the final state of the system, taking into account the free evolution after the cessation of external influence.

Second, in Fig. 7 we show a significant influence of the phase incursion on the process of the non-adiabatic Landau–Zener transition during the evolution of the state vector of the system from the moment of the onset of the magnetic flux input at $t = 0$ to the moment of the first level anticrossing, at $t = t_1$, which is marked by the dotted line in Fig. 4a. Consequently, by optimizing these two parameters, i.e. the rise, t_1, and full t_2 times of the input magnetic flux in (1), we need to obtain a complete coverage of the Bloch sphere (see Fig. 7c), taking into account the free precession around the z axis. The uneven density of the coverage points is related to the properties of the rotation of the eigenvectors on the Bloch sphere, determined by the speed of passage of the anti-crossing areas for the energy levels [53].

The final stage of the work was to optimize the shape of the external control action (choice of time $t_{1,2}$ and speed of action D_1) for a given energy landscape of the AQFP cell to demonstrate the implementation of quantum operations. In Fig. 8, the colors indicate the areas on the parameter plane for high-quality quantum operations. The mentioned quality was calculated based on the fidelity metric [55]:

$$F_{op} = \frac{Tr\hat{U}^{\dagger}\hat{U} + |Tr(\hat{U}^{\dagger}\hat{U}_{id})|^2}{d(d+1)}, \tag{10}$$

where $\hat{U} = \hat{T}e^{-i\int_0^t \hat{H}(\tau)d\tau}$ is the evolution operator for the numerical solution of the Schrodinger equation, and $\hat{U}_{id}$ is the ideal operation matrix, $d = 2$ is the dimension of the system, $\hat{T}$ is the time-ordering operator.

We calculated the fidelity for the following set of basic operations, op [56]: state inversion NOT (gate X), phase inversion (gate Z), Hadamard gate (H), and combinations of gates HZ. It can be seen that for each of these gates, regions of control action can be found to perform a high-precision quantum operation with a value of $F_{op} > 0.9999$.

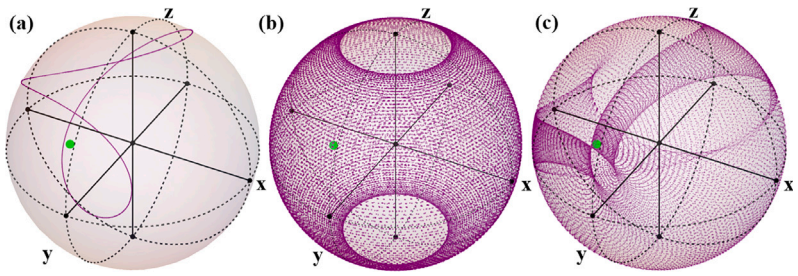

Fig. 7. The purple points on the Bloch sphere correspond to the set of possible final states after the application of the unipolar control signal φ_{in_1}, with variation of only the time t_2 (a), rotation of these points around z-axis (b), and simultaneous variation of the rise time t_1 and the fall time t_2 (c). The initial state is marked on the Bloch spheres with the green point. Other parameters are: $l_1 = 1.98,\ l_2 = 1.82,\ l_{out} = 1.92,\ D_1 = 0.01425$.

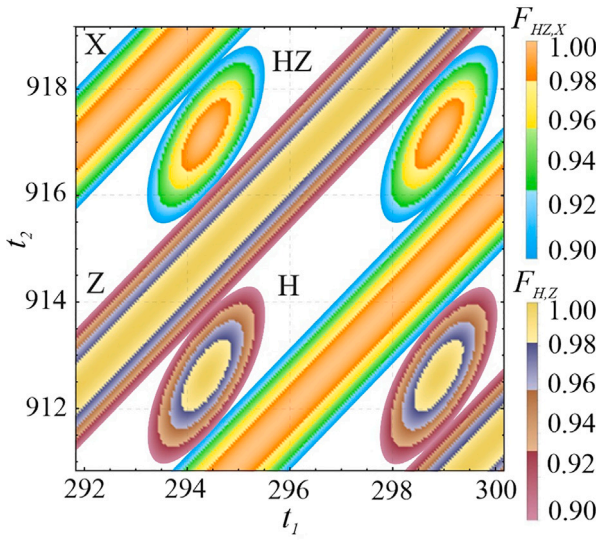

Fig. 8. The color on the map of control action parameters $t_{1,2}$ shows the fidelity values F_{op} for performing gate operations from the set described in the text: $op = \{X, Z, H, HZ\}$. For better differentiation of the operation ranges, only those parameter ranges with a fidelity greater than 0.9 are shown. Other parameters are: $l_1 = 1.98,\ l_2 = 1.82,\ l_{out} = 1.92,\ D_1 = 0.01425$.

4. Discussion and conclusion

A characteristic feature of systems with flying qubits is the ability to convert states of stationary qubits into states moving in space (flying) and states of flying qubits into states of stationary qubits. In the traditional approach, to work with solid-state stationary qubits and photons as flying qubits, three main problems have to be solved: generation, reception, and conversion [57]. The advantage of the AQFP is that it can act both as a stationary qubit [58–60] and operate as a component of a chain of coupled nonlinear oscillators in which there can exist excitations propagating in space in the form of current and phase waves of the superconducting order parameter, playing the role of flying qubits. The presence of a shunt inductor in the interferometer and the adiabatic dynamics during the potential evolution allow to avoid transitions of Josephson junctions into a resistive state. This leads to very low energy dissipation and, in the limit, to the formation of a "potential valley" through which the system oscillates from one logical state to another. Logical states of the system correspond to certain aforementioned excitations (mutual directions of circulating currents) in it. The described properties of the system allow to consider it in the quantum regime (the distances between the energy levels are much larger than the energy of thermal fluctuations and "dissipative" broadening) as a "flying qubit", whose states are now associated with superpositions of different circulating currents.

These excitations, carefully transferred by "gentle hands" of the adiabatic potential of the parametron, flying from one AQFP to the next in the chain, carry information from one quantum system to another. Besides, these quantum systems can be located within the limits of one chip or several. This approach allows one to naturally transfer the state of a stationary qubit to the state of a flying qubit and vice versa, and at the same time to solve the problems of detection of a flying qubit and its processing. The further development of the idea proposed here will be devoted precisely to the study of logic state transfer over an AQFP-based quantum data bus, as well as taking into account the influence of thermal noise [61–63] on the dynamics of ongoing processes in the system.

In this work we have shown that in AQFP-based systems with flying qubits one can avoid using bulky waveguides for controlling quantum states. This is possible by choosing the level, duration, and shape of the control unipolar magnetic flux pulses generated by adiabatic superconducting electronics [64] that ensures the population of the required energy level of the target qubit with leakage into undesired states of less than 10^{-4}. It has also been demonstrated that the controlled asymmetry in the AQFP allows to realize a full set of operations over the cell in a quantum data bus.

CRediT authorship contribution statement

M.V. Bastrakova: Writing – original draft, Methodology, Investigation, Data curation. **D.S. Pashin:** Visualization, Software, Methodology, Investigation. **P.V. Pikunov:** Methodology, Investigation. **I.I. Soloviev:** Writing – review & editing, Supervision, Formal analysis. **A.E. Schegolev:** Writing – original draft, Visualization, Investigation, Data curation, Conceptualization. **N.V. Klenov:** Writing – review & editing, Writing – original draft, Project administration, Funding acquisition, Data curation, Conceptualization.

Declaration of competing interest

The authors declare the following financial interests/personal relationships which may be considered as potential competing interests: M. V. Bastrakova reports financial support was provided by Russian Science Foundation. If there are other authors, they declare that they have no known competing financial interests or personal relationships that could have appeared to influence the work reported in this paper.

Acknowledgments

The development of the main concept was supported by the Ministry of Science and Higher Education of the Russian Federation (agreement No. 075-15-2024-632). The development of the method of analysis for the development of adiabatic logic cells was carried out with the support of the Grant of the Russian Science Foundation 22-72-10075. A.S. is grateful for the grant 22-1-3-16-1 of the Foundation for the Advancement of Theoretical Physics and Mathematics "BASIS". M.B. was supported by Rosatom within the framework of the Roadmap for Quantum Computing (Contract No. 868-1.3-15/15-2021 dated October 5).

Data availability

Data will be made available on request.

References

[1] Yan F, Gustavsson S, Kamal A, Birenbaum J, Sears AP, Hover D, Gudmundsen TJ, Rosenberg D, Samach G, Weber S, et al. The flux qubit revisited to enhance coherence and reproducibility. Nat Commun 2016;7(1):12964.

[2] Ivić Z, Lazarides N, Tsironis GP. Self-induced transparency in a flux-qubit chain. Chaos, Solitons Fractals X 2019;1:100003.

[3] Dmitriev AY, Astafiev O. A perspective on superconducting flux qubits. Appl Phys Lett 2021;119(8):080501.

[4] Bastrakova MV, Klenov NV, Ruzhickiy VI, Soloviev II, Satanin AM. Sub-nanosecond operations on superconducting quantum register based on Ramsey patterns. Supercond Sci Technol 2022;35(5):055003. http://dx.doi.org/10.1088/1361-6668/ac5505.

[5] Chang T, Holzman I, Cohen T, Johnson B, Jamieson D, Stern M. Reproducibility and gap control of superconducting flux qubits. Phys Rev Appl 2022;18(6):064062.

[6] Somoroff A, Ficheux Q, Mencia RA, Xiong H, Kuzmin R, Manucharyan VE. Millisecond coherence in a superconducting qubit. Phys Rev Lett 2023;130(26):267001.

[7] Kalacheva D, Fedorov G, Zotova J, Kadyrmetov S, Kirkovskii A, Dmitriev A, Astafiev O. Kinemon: An inductively shunted transmon artificial atom. Phys Rev Appl 2024;21:024058. http://dx.doi.org/10.1103/PhysRevApplied.21.024058, URL https://link.aps.org/doi/10.1103/PhysRevApplied.21.024058.

[8] Likharev K. Dynamics of some single flux quantum devices: I. Parametric quantron. IEEE Trans Magn 1977;13(1):242–4.

[9] Hosoya M, Hioe W, Casas J, Kamikawai R, Harada Y, Wada Y, Nakane H, Suda R, Goto E. Quantum flux parametron: A single quantum flux device for josephson supercomputer. IEEE Trans Appl Supercond 1991;1(2):77–89.

[10] Takeuchi N, Ehara K, Inoue K, Yamanashi Y, Yoshikawa N. Margin and energy dissipation of adiabatic quantum-flux-parametron logic at finite temperature. IEEE Trans Appl Supercond 2013;23(3):1700304. http://dx.doi.org/10.1109/TASC.2012.2232336.

[11] Takeuchi N, Ozawa D, Yamanashi Y, Yoshikawa N. An adiabatic quantum flux parametron as an ultra-low-power logic device. Supercond Sci Technol 2013;26(3):035010. http://dx.doi.org/10.1088/0953-2048/26/3/035010.

[12] Takeuchi N, Yamanashi Y, Yoshikawa N. Measurement of 10 zj energy dissipation of adiabatic quantum-flux-parametron logic using a superconducting resonator. Appl Phys Lett 2013;102(5):052602. http://dx.doi.org/10.1063/1.4790276, arXiv:https://pubs.aip.org/aip/apl/article-pdf/doi/10.1063/1.4790276/14279427/052602_1_online.pdf.

[13] Ayala CL, Tanaka T, Saito R, Nozoe M, Takeuchi N, Yoshikawa N. Mana: A monolithic adiabatic integration architecture microprocessor using 1.4-zj/op unshunted superconductor josephson junction devices. IEEE J Solid-State Circuits 2020;56(4):1152–65.

[14] Takeuchi N, Yamae T, Ayala CL, Suzuki H, Yoshikawa N. Adiabatic quantum-flux-parametron: A tutorial review. IEICE Trans Electron 2022;105(6):251–63.

[15] Luo W, Chen O, Yoshikawa N, Takeuchi N. Scalable true random number generator using adiabatic superconductor logic. Sci Rep 2022;12(1):20039.

[16] Yamae T, Takeuchi N, Yoshikawa N. An adiabatic quantum-flux-parametron 8-bit ripple carry adder using delay-line clocking. IEEE Trans Appl Supercond 2023;33(5):1–4.

[17] Schegolev A, Klenov N, Soloviev I, Tereshonok M. Learning cell for superconducting neural networks. Supercond Sci Technol 2020;34(1):015006.

[18] Schegolev AE, Klenov NV, Bakurskiy SV, Soloviev II, Kupriyanov MY, Tereshonok MV, Sidorenko AS. Tunable superconducting neurons for networks based on radial basis functions. Beilstein J Nanotechnol 2022;13(1):444–54.

[19] Bastrakova MV, Pashin DS, Rybin DA, Schegolev AE, Klenov NV, Soloviev II, Gorchavkina AA, Satanin AM. A superconducting adiabatic neuron in a quantum regime. Beilstein J Nanotechnol 2022;13:653–65. http://dx.doi.org/10.3762/bjnano.13.57.

[20] Ionin A, Karelina L, Shuravin N, Sidel'nikov M, Razorenov F, Egorov S, Bol'ginov V. Experimental study of the transfer function of a superconducting Gauss neuron prototype. JETP Lett 2023;118(10):766–72.

[21] Luo W, Chen O, Yoshikawa N, Takeuchi N. Sigmoid function generator using stochastic adiabatic superconductor logic. Appl Phys Lett 2023;122(24).

[22] Pashin DS, Bastrakova MV, Rybin DA, Soloviev II, Klenov NV, Schegolev AE. Optimisation challenge for a superconducting adiabatic neural network that implements XOR and OR boolean functions. Nanomaterials 2024;14(10):854. http://dx.doi.org/10.3390/nano14100854.

[23] Yamauchi T, Takeuchi N, Yoshikawa N, San H, Chen O. Dual-mode neuron design with deterministic and non-deterministic operations using adiabatic superconductor devices. Supercond Sci Technol 2024.

[24] Takeuchi N, Yamae T, Luo W, Hirayama F, Yamamoto T, Yoshikawa N. Scalable flux controllers using adiabatic superconductor logic for quantum processors. Phys Rev Res 2023;5(1):013145.

[25] Takeuchi N, Yamae T, Yamashita T, Yamamoto T, Yoshikawa N. Microwave-multiplexed qubit controller using adiabatic superconductor logic. Npj Quantum Inf 2024;10(1):53.

[26] Di Palma L, Miano A, Mastrovito P, Massarotti D, Arzeo M, Pepe G, Tafuri F, Mukhanov O. Discriminating the phase of a coherent tone with a flux-switchable superconducting circuit. Phys Rev Appl 2023;19:064025. http://dx.doi.org/10.1103/PhysRevApplied.19.064025, URL https://link.aps.org/doi/10.1103/PhysRevApplied.19.064025.

[27] Gulevich D, Gaifullin M, Kusmartsev F. Controlled dynamics of sine-Gordon breather in long josephson junctions. PEur. Phys J B 2012;85:24.

[28] De Santis D, Guarcello C, Spagnolo B, Carollo A, Valenti D. Generation of travelling sine-Gordon breathers in noisy long josephson junctions. Chaos Solitons Fractals 2022;158:112039. http://dx.doi.org/10.1016/j.chaos.2022.112039, URL https://www.sciencedirect.com/science/article/pii/S0960077922002491.

[29] De Santis D, Guarcello C, Spagnolo B, Carollo A, Valenti D. Supratransmission-induced traveling breathers in long josephson junctions. Commun Nonlinear Sci Numer Simul 2022;115:106736. http://dx.doi.org/10.1016/j.cnsns.2022.106736, URL https://www.sciencedirect.com/science/article/pii/S100757042200274X.

[30] De Santis D, Guarcello C, Spagnolo B, Carollo A, Valenti D. Breather dynamics in a stochastic sine-Gordon equation: Evidence of noise-enhanced stability. Chaos Solitons Fractals 2023;168:113115. http://dx.doi.org/10.1016/j.chaos.2023.113115, URL https://www.sciencedirect.com/science/article/pii/S0960077923000164.

[31] De Santis D, Guarcello C, Spagnolo B, Carollo A, Valenti D. Ac-locking of thermally-induced sine-Gordon breathers. Chaos Solitons Fractals 2023;170:113382. http://dx.doi.org/10.1016/j.chaos.2023.113382, URL https://www.sciencedirect.com/science/article/pii/S0960077923002837.

[32] De Santis D, Guarcello C, Spagnolo B, Carollo A, Valenti D. Noise-induced, ac-stabilized sine-Gordon breathers: Emergence and statistics. Commun Nonlinear Sci Numer Simul 2024;131:107796. http://dx.doi.org/10.1016/j.cnsns.2023.107796, URL https://www.sciencedirect.com/science/article/pii/S1007570423007177.

[33] Di Fresco G, De Santis D, Guarcello C, Spagnolo B, Carollo A, Valenti D. Effects of correlated noise on the excitation of robust breathers in an ac-driven, lossy sine–Gordon system. Chaos Solitons Fractals 2024;189:115678. http://dx.doi.org/10.1016/j.chaos.2024.115678, URL https://www.sciencedirect.com/science/article/pii/S096007792401230X.

[34] Likharev KK. Classical and quantum limitations on energy consumption in computation. Internat J Theoret Phys 1982;21:311–26.

[35] Semenov VK, Danilov GV, Averin DV. Classical and quantum operation modes of the reversible josephson-junction logic circuits. IEEE Trans Appl Supercond 2007;17(2):455–61.

[36] Ren J, Semenov VK, Polyakov YA, Averin DV, Tsai J-S. Progress towards reversible computing with nSQUID arrays. IEEE Trans Appl Supercond 2009;19(3):961–7.

[37] Ren J, Semenov VK. Progress with physically and logically reversible superconducting digital circuits. IEEE Trans Appl Supercond 2011;21(3):780–6.

[38] Takeuchi N, Yamanashi Y, Yoshikawa N. Reversible logic gate using adiabatic superconducting devices. Sci Rep 2014;4(1):1–4.

[39] Pekola J, Golubev D, Averin D. Maxwell's demon based on a single qubit. Phys Rev B 2016;93(2):024501.

[40] Fujii T, Shibata T, Nishida M, Hatakenaka N. Flying superconducting qubits. IEEE Trans Appl Supercond 2007;17(2):97–100. http://dx.doi.org/10.1109/TASC.2007.898035.

[41] Fujii T, Nishida M, Hatakenaka N. Mobile qubits in quantum josephson circuits. Phys Rev B 2008;77:024505. http://dx.doi.org/10.1103/PhysRevB.77.024505, URL https://link.aps.org/doi/10.1103/PhysRevB.77.024505.

[42] Tolpygo SK, Golden EB, Ayala CL, Schindler L, Johnston MA, Parmar N, Yoshikawa N. Characterization of adiabatic quantum-flux-parametrons in the MIT LL SFQ5ee+ process. 2024, arXiv:2411.04045.

[43] Rower DA, Ding L, Zhang H, Hays M, An J, Harrington PM, Rosen IT, Gertler JM, Hazard TM, Niedzielski BM, Schwartz ME, Gustavsson S, Serniak K, Grover JA, Oliver WD. Suppressing counter-rotating errors for fast single-qubit gates with fluxonium. 2024, arXiv:2406.08295.

[44] Landau LD. A theory of energy transfer. II. Phys Z. Sowjetunion 1932;2:46.

[45] Zener C. Non-adiabatic crossing of energy levels. Proc R Soc A 1932;137:696–702.

[46] Stückelberg ECG. Theory of inelastic collisions between atoms. Helv Phys Acta 1932;5:369–423.

[47] Oliver WD, Yu Y, Lee JC, Berggren KK, Levitov LS, Orlando TP. Mach-zehnder interferometry in a strongly driven superconducting qubit. Science 2005;310(5754):1653–7. http://dx.doi.org/10.1126/science.1119678, arXiv:https://www.science.org/doi/pdf/10.1126/science.1119678.

[48] Gaudreau L, Granger G, Kam A, Aers GC, Studenikin SA, Zawadzki P, Pioro-Ladrière M, Wasilewski ZR, Sachrajda AS. Coherent control of three-spin states in a triple quantum dot. Nat Phys 2012;8:54—-58.

[49] Cao G, Li H-O, Tu T, Wang L, Zhou C, Xiao M, Guo G-C, Jiang H-W, Guo G-P. Coherent control of three-spin states in a triple quantum dot. Nat Commun 2013;4:1401.

[50] Pashin DS, Pikunov PV, Bastrakova MV, Schegolev AE, Klenov NV, Soloviev II. A bifunctional superconducting cell as flux qubit and neuron. Beilstein J Nanotechnol 2023;14:1116–26. http://dx.doi.org/10.3762/bjnano.14.92.

[51] Shevchenko SN, Ashhab S, Nori F. Landau–Zener–Stückelberg interferometry. Phys Rep 2010;492(1):1–30.

[52] Ivakhnenko V, Shevchenko SN, Nori F. Nonadiabatic Landau–Zener–Stückelberg–Majorana transitions, dynamics, and interference. Phys Rep 2023;995:1–89.

[53] Ryzhov A, Ivakhnenko O, Shevchenko S, Gonzalez-Zalba M, Nori F. Alternative fast quantum logic gates using nonadiabatic Landau-Zener-Stückelberg-Majorana transitions. Phys Rev Res 2024;6(3):033340.

[54] Lemaréchal C. Cauchy and the gradient method. Doc Math Extra 2012;251–4.

[55] Pedersen LH, Møller NM, Mølmer K. Fidelity of quantum operations. Phys Lett A 2007;367(1):47–51. http://dx.doi.org/10.1016/j.physleta.2007.02.069, URL https://www.sciencedirect.com/science/article/pii/S0375960107003271.

[56] Kaye P, Laflamme R, Mosca M. An Introduction to Quantum Computing. Oxford, England: Oxford University Press UK; 2006.

[57] Li W, Sun H, Liu Y, Li T, Wu R-B. Flying-qubit control: Basics, progress, and outlook. Adv Devices & Instrum 2024;5:0059.

[58] Chancellor N, McGeoch CC, Mniszewski S, Bernal Niera D. Experience with quantum annealing computation. Front Comput Sci 2024;6:1481330.

[59] King AD, Nocera A, Rams MM, Dziarmaga J, Wiersema R, Bernoudy W, Raymond J, Kaushal N, Heinsdorf N, Harris R, et al. Computational supremacy in quantum simulation. 2024, arXiv preprint arXiv:2403.00910.

[60] Irbäck A, Knuthson L, Mohanty S, Peterson C. Using quantum annealing to design lattice proteins. Phys Rev Res 2024;6(1):013162.

[61] Grimaudo R, Valenti D, Filatrella G, Spagnolo B, Guarcello C. Coupled quantum pendula as a possible model for josephson-junction-based axion detection. Chaos Solitons Fractals 2023;173:113745. http://dx.doi.org/10.1016/j.chaos.2023.113745, URL https://www.sciencedirect.com/science/article/pii/S096007792300646X.

[62] Grimaudo R, Valenti D, Spagnolo B, Filatrella G, Guarcello C. Josephson-junction-based axion detection through resonant activation. Phys Rev D 2022;105:033007. http://dx.doi.org/10.1103/PhysRevD.105.033007, URL https://link.aps.org/doi/10.1103/PhysRevD.105.033007.

[63] Guarcello C. Lévy noise effects on josephson junctions. Chaos Solitons Fractals 2021;153:111531. http://dx.doi.org/10.1016/j.chaos.2021.111531, URL https://www.sciencedirect.com/science/article/pii/S0960077921008857.

[64] Vozhakov VA, Bastrakova MV, Klenov NV, Soloviev II, Pogosov WV, Babukhin DV, Zhukov AA, Satanin AM. State control in superconducting quantum processors. Phys- Uspekhi 2022;65:457–76.